Neferine promotes the apoptosis of HNSCC through the accumulation of p62/SQSTM1 caused by autophagic flux inhibition

FENGSHUO ZHU[1*], XIAOGUANG LI[1*], XIAO TANG[1], JUNJIAN JIANG[1], YU HAN[1], YINUO LI[2], CHUNYUE MA[1], ZHONGLONG LIU[1] and YUE HE[1]

[1]Department of Oral Maxillofacial-Head and Neck Oncology, Shanghai Ninth People's Hospital, College of Stomatology, Shanghai Jiao Tong University School of Medicine, National Clinical Research Center for Oral Disease, Shanghai Key Laboratory of Stomatology and Shanghai Research Institute of Stomatology, Shanghai 200011, P.R. China; [2]Department of Pathology, Feinberg School of Medicine, Northwestern University, Chicago, IL 60611, USA

Received August 6, 2020; Accepted April 2, 2021

DOI: 10.3892/ijmm.2021.4957

Abstract. Head and neck squamous cell carcinoma (HNSCC), one of the most common malignancies worldwide, often has a poor prognosis due to the associated metastasis and chemoresistance. Hence, the development of more effective chemotherapeutics is critical. Neferine, a bisbenzylisoquinoline alkaloid isolated from the seed embryo of *Nelumbo nucifera* (common name: Lotus), exerts antitumor effects by regulating apoptosis and autophagy pathways, making it a potential therapeutic option for HNSCC. In our study, it was revealed that neferine inhibited the growth and induced the apoptosis of HNSCC cells both *in vitro* and *in vivo*. Furthermore, the results revealed that neferine activated the ASK1/JNK pathway by increasing reactive oxygen species production, resulting in the subsequent induction of apoptosis and the regulation of canonical autophagy in HNSCC cells. Moreover, a novel pro-apoptotic mechanism was described for neferine via the activation of caspase-8 following the accumulation of p62, which was caused by autophagic flux inhibition. These findings provided insights into the mechanisms responsible for the anticancer effect of neferine, specifically highlighting the crosstalk that occured between apoptosis and autophagy, which was mediated by p62 in HNSCC. Hence, the neferine-induced inhibition of autophagic flux may serve as the basis for a potential adjuvant therapy for HNSCC.

Correspondence to: Dr Yue He or Dr Zhonglong Liu, Department of Oral Maxillofacial-Head and Neck Oncology, Shanghai Ninth People's Hospital, College of Stomatology, Shanghai Jiao Tong University School of Medicine, National Clinical Research Center for Oral Disease, Shanghai Key Laboratory of Stomatology and Shanghai Research Institute of Stomatology, 639 Zhi Zao Ju Road, Shanghai 200011, P.R. China
E-mail: heyuejiuyuan@163.com
E-mail: eddielew021@163.com

*Contributed equally

Key words: neferine, apoptosis, autophagy, head and neck squamous cell carcinoma

Introduction

Head and neck squamous cell carcinoma (HNSCC) originates from the mucosal surfaces of the oral cavity, oropharynx, larynx, and hypopharynx, accounting for more than 90% of the cancers of the head and neck (1). As the sixth most common cancer worldwide, HNSCC is highly aggressive and characterized by complex genetic alterations, and current treatment options for HNSCC consist of surgical interventions, radiotherapy, and chemotherapy (2,3). Although a number of advances have been made in these modalities, the recurrence rate remains high owing to the development of chemotherapy resistance, resulting in a low overall patient survival rate (4,5). Therefore, the identification of novel chemotherapeutic agents is urgently needed to prevent cancer recurrence and delay cancer progression.

Compounds derived from plants have significantly contributed to the development of novel anticancer therapeutics. *Nelumbo nucifera* (common name: Lotus) is widely used in Indian and Chinese medicine for cardiovascular (6) and pulmonary (7) diseases as well as nervous system-related disorders (8). In addition, neferine, the major bisbenzylisoquinoline alkaloid isolated from the seed embryo of the lotus, has recently been revealed to exert antitumor effects through various pathways. For instance, neferine reportedly inhibited the proliferation and growth of prostate cancer cell (9), osteosarcoma (10), hepatocellular carcinoma (11), and lung cancer cells (12). Neferine also exhibited the ability to suppress the migration of gastrointestinal stromal tumor cells (13) and glioma cells (14). Furthermore, recent research suggests that neferine induces autophagy (15) and inhibits ovarian cancer cell angiogenesis (16). However, the effects of neferine on HNSCC have not yet been elucidated.

Macroautophagy is a major intracellular catabolic mechanism that directs the degradation of cytoplasmic components and organelles in the lysosome (17) that can

have cytoprotective or cytopathic roles in response to various stresses, including therapeutic stress. Autophagic flux denotes the complete process of autophagy, including autophagosome biogenesis, maturation, fusion with lysosomes, and the breakdown of autophagic substrates inside the lysosome (18). Indeed, autophagic flux induction or inhibition using natural compounds has shown promise in the treatment of diseases such as cancer (19). Additionally, apoptosis, another critical catabolic pathway essential for the cellular response to toxic agents, participates in extensive crosstalk with autophagy (20), rendering both pathways crucial for the development of effective cancer therapeutics.

Therefore, in the present study, HNSCC cell lines and a xenograft mouse model were used to investigate the antitumor mechanism of neferine between autophagy and apoptosis, with the aim of presenting a promising alternative therapeutic agent for HNSCC.

Materials and methods

Cell lines and culture. The HNSCC cell lines used in the present study were HN6 (tongue squamous cell carcinoma; provided by the Shanghai Ninth People's Hospital, Shanghai, China), HN30 (pharyngeal squamous cell carcinoma; provided by the University of Maryland School of Dentistry, Maryland, USA) and Cal27 (tongue squamous cell carcinoma; purchased from ATCC). The control cell line was the human immortalized oral epithelial cell line (HIOEC), which was established by the Shanghai Ninth People's Hospital (21). All cell lines were cultured in Dulbecco's modified Eagle's medium (DMEM; Gibco; Thermo Fisher Scientific, Inc.) supplemented with 10% fetal bovine serum (FBS) and 1% penicillin-streptomycin (Gibco; Thermo Fisher Scientific, Inc.). Cells were cultured in a humidified atmosphere containing 5% CO_2 at 37˚C.

Cell proliferation assay. Cell viability was determined using the Cell Counting Kit-8 (CCK-8) assay kit (Dojindo Molecular Technologies, inc.). Briefly, HN6, HN30 and CAL27 cells were seeded at a density of $5x10^3$ cells/well in a 96-well plate, with 200 μl DMEM medium (10% FBS). After incubation with indicated concentrations of neferine (0, 7.5, 15, 22.5 and 30 μM; MCE), 10 μl CCK-8 reagent was added to each well, and the absorbance was measured at 450 nm after 2 h of incubation at 37˚C in the incubator. All experiments were repeated in triplicate.

Clonogenic assay. For the clonogenic assay, HN6, HN30 and CAL27 single-cell suspensions were prepared. A total of 500 cells were seeded/well in 6-well plates at 37˚C overnight. The cells were treated with various concentrations (0, 1, 2, 5 and 10 μM) of neferine for 2 weeks. Cell colonies were fixed with pure methanol for 15 min and stained with 0.1% crystal violet (Beyotime Biotechnology) for 30 min at room temperature. The images were captured and scored with CanoScan 5600F (Canon, Inc.). Colonies of >50 cells were counted to determine the surviving fraction. All experiments were repeated in triplicate.

Cell cycle analysis. Single-cell suspensions were prepared, and $3x10^5$ cells were seeded per well in 6-well plates overnight in the cell incubator. After treatment with various concentrations of neferine (0, 5, 10, 15 and 20 μM) for 24 h, HN6, HN30 and CAL27 cells were collected and fixed in 3 ml cold 75% ethanol at -20˚C overnight. After washing with 2 ml of cold PBS, the cells were resuspended and incubated with 0.5 ml of PBS containing 100 μg/ml RNase (Beyotime Biotechnology) and 5 μg/ml propidium iodide (Shanghai Yeasen Biotechnology Co., Ltd.) at room temperature for 30 min. The cell cycle distribution was analyzed via BD FACSCalibur flow cytometer (BD Biosciences) and ModFIT 5.0 software (Verity Software House, Inc.).

Annexin V apoptosis assay. Apoptotic cells were identified using the FITC Annexin V Apoptosis Detection Kit (BD Biosciences). A total of $3x10^5$ cells were seeded per well in 6-well plates overnight in the cell incubator. After treatment with the indicated concentrations (0, 5, 10, 15 and 20 μM) of neferine for 48 h, the cells were resuspended in binding buffer. FITC Annexin V (5 μl) and PI (5 μl) were then added and were incubated at room temperature for 15 min in the dark. Apoptotic cells were analyzed via BD FACSCalibur flow cytometer and FlowJo (V10) software (BD Biosciences).

Reactive oxygen species (ROS) assay. Intracellular ROS levels were determined using the DCFH-DA fluorescent probe (Beyotime Biotechnology). Briefly, $3x10^5$ cells were seeded per cell in 6-well plates overnight in the cell incubator. After treatment with the indicated concentrations of neferine (0, 5, 10 and 20 μM) for 12 h, HN6, HN30 and CAL27 cells were incubated with DCFH-DA for 30 min in the cell incubator. Dichlorofluorescein (DCF) fluorescence was then detected via BD FACSCalibur flow cytometer (FITC-channel). Fluorescence microscopy (magnification, x100; Carl Zeiss AG) was used to capture images of the cells.

Cell migration assay. The cell migration assay was performed using the Transwell system (24-wells, 8-μm pore size with polycarbonate membrane; Corning Costar; Corning, Inc.). HN30 and CAL27 cells were suspended in serum-free medium ($5.0x10^5$/ml), and 100 μl was added to the upper chamber, whereas 600 μl of complete medium (10% FBS) was added to the lower chamber. After 4 h, the media in the upper chamber was replaced with media containing various concentrations of neferine (0, 5, 10 and 20 μM, serum-free). After 36 h, the chambers were fixed with 4% paraformaldehyde for 15 min and stained with 0.1% crystal violet for 30 min at room temperature. The non-migrated cells were wiped from the upper surface of the chamber using cotton swabs. The successfully migrated cells were counted in three random fields using a light microscope (magnification, x40; Olympus Corporation).

Scratch assay. Scratch assays were applied to determine cell mobility. First, $1x10^6$ HN6, HN30 and CAL27 cells were seeded per well in a 6-well plate in complete medium overnight in the cell incubator to obtain a fully confluent monolayer. After 12 h of starvation with DMEM (serum-free), a 20-μl pipette tip was used to make a straight cell-free 'scratch' in each well. The cells were washed with PBS, and serum-free medium was added with various concentrations

of neferine (0, 5, 10, 15 and 20 μM). Finally, the migration of the cells was captured using a phase contrast microscope (magnification, x100; Olympus Corporation). Images of cells were obtained at the matching reference points initially and then at 12-h intervals. The wound closure of the scratch was analyzed quantitatively.

Western blot analysis. Briefly, HN6, HN30 and CAL27 cells were collected after specific treatments and lysed with RIPA buffer (Beyotime Biotechnology). The protein concentration was measured using the Pierce BCA Protein Assay Kit (Thermo Fisher Scientific, Inc.). A total of 20 μg protein in each sample was run on 10% SDS-PAGE gels and then electro-transferred onto a PVDF membrane (EMD Millipore). The membrane was blocked with 5% skimmed milk for 1 h at room temperature and incubated overnight with primary antibodies (1:1,000) at 4˚C. The membrane was washed and incubated with HRP-conjugated secondary antibodies [cat. nos. 70-GAR0072 and 70-GAM0072; 1:5,000; Multi Sciences (LIANKE) Biotech, Co., Ltd.] for 1 h at the room temperature. Protein bands were then detected using a chemiluminescence system (Immobilion Western Chemiluminescent HRP Substrate; EMD Millipore). All bands were quantified using ImageJ V1.8. β-Actin was used as an internal control. The primary antibodies were as follows: Anti-cleaved caspase-3 (product no. 9664; Cell Signaling Technology, Inc.; and cat. no. sc-7272; Santa Cruz Biotechnology, Inc.), anti-cleaved caspase-9 (cat. no. 10380-1-AP), anti-cleaved PARP1 (cat. no. 13371-1-AP), anti-Beclin-1 (cat. no. 11306-1-AP) and anti-p62 (cat. no. 18420-1-AP) (all from ProteinTech Group, Inc.), anti-BAX (cat. no. AF0054) and anti-β-Actin (cat. no. AF0003) (both from Beyotime Biotechnology); anti-Bcl-2 (cat. no. sc-7382; Santa Cruz Biotechnology, Inc.), and anti-LC3-I/II (product code 128025; Abcam Inc.).

Transmission electron microscopy (TEM) assay. After neferine treatment (0 and 20 μM) for 24 h in the cell incubator, HN30 and CAL27 cells were fixed with 2.5% glutaraldehyde for 4 h and 1% OsO_4 (Solarbio Life Science) for 1 h at 4˚C, dehydrated with graded ethanol, embedded in propylene oxide, sectioned at 70 nm and stained with 2% uranyl acetate (Sigma-Aldrich; Merck KGaA) for 20 min at room temperature. The autophagosomes were visualized using electron microscopy, as previously described (22,23).

Fluorescence imaging. HN30 and CAL27 cells were seeded in 6-well plates overnight in the cell incubator and then transfected with GFP-RFP-LC3 adenovirus (10^8 pfu/ml MOI=10; Beyotime Biotechnology). After 24 h in the cell incubator, the medium was removed and replaced with the indicated treatments [neferine 10 μM, 24 h; EBSS (cat. no. E2888; Sigma Aldrich; Merck KGaA), 6 h; chloroquine (MCE) 10 μM, 24 h]. Autophagic flux was measured via fluorescence microscopy (magnification x400; Carl Zeiss AG).

RNA interference. The sequence for the small interfering (si)RNA against p62 was 5'-GCATTGAAGTTGATATCG AT-3' (24). The non-targeting siRNA control was obtained from Dharmacon, Inc. CAL27 cells ($3x10^5$) were seeded per well in a 6-well plate and transfected with siRNA (75 pmol) using Lipofectamine 3000 (Invitrogen; Thermo Fisher Scientific, Inc.) for 12 h in the cell incubator. After 72 h, the transfected cells were used for the neferine experiments.

Xenograft mouse model. The animal experiments were approved by the Ethics Review Board at the Shanghai Ninth People's Hospital (Shanghai, China). CAL27 cells ($2x10^6$) suspended in 20% Matrigel (BD Biosciences) were subcutaneously injected into the dorsa of five-week-old male BALB/c nude mice (Vital River, Inc.; Charles River Laboratories, Inc.) in routine living and feeding conditions (temperature 24±2˚C, humidity 40-60%, 12-h light/dark cycle, sterile feed and filtered water *ad libitum*). After 1 week, ten mice (tumors had formed) were randomly divided into two groups (5 mice per group). The mice were administered neferine (10 mg/kg) or PBS (control) intraperitoneally. The tumor volume was measured every 4 days ($V=LengthxWidth^2x0.5$). The humane endpoints were as follows: i) maximum tumor volume 1,000 mm^3; ii) tumor ulceration or necrosis. The mice were anesthetized with diethyl ether, then euthanized by cervical dislocation. A combination of criteria in confirming death included lack of pulse, breathing, corneal reflex, and response to firm toe pinch.

Immunohistochemical staining. Tissues were fixed with 4% paraformaldehyde for 24 h at 4˚C and dehydrated and embedded in paraffin. The paraffin sections (4 μm) were deparaffinized, rehydrated and subjected to antigen reparation (microwave oven, 6 min x 4 times), endogenous peroxidase inactivation (0.3% H_2O_2, 15 min), and nonspecific antigen blocking (FBS; Gibco; Thermo Fisher Scientific, Inc.) for 15 min, at room temperature. The slides were then incubated with primary antibodies overnight (4˚C) and, subsequently, with a secondary antibody for 15 min (at room temperature). Staining was detected using a diaminobenzidine (DAB) reagent (Zhongshan Jinqiao; ZSGB-BIO, Inc.) for 1 min at room temperature. The intensity and proportion of staining were scored by two pathologists with an Olympus light microscope (magnification, x200). The primary antibodies were as follows: Anti-cleaved caspase-3 (product no. 9664; 1:1,000; Cell Signaling Technology, Inc.); anti-cleaved PARP1 (cat. no. 13371-1-AP; 1:200), anti-Ki67 (cat. no. 10205-2-AP; 1:500), anti-LC3 (cat. no. 14600-1-AP; 1:400) and anti-p62 (cat. no. 18420-1-AP; 1:50) (all from ProteinTech Group, Inc.). The secondary antibody was as follows: HRP-conjugated [cat. no. 70-GAR0072; 1:1,000; Multi Sciences(LIANKE) Biotech, Co., Ltd.].

Statistical analysis. Statistical comparisons between two groups were performed using non-paired Student's t-test. Statistical comparisons between multiple groups were performed by Tukey's post hoc test with one-way ANOVA. SPSS version 18.0 software (SPSS, Inc.) was used for statistical analysis. For each of the three independent experiments, the data are presented as the mean ± SEM. $P<0.05$ was considered to indicate a statistically significant difference.

Results

Neferine inhibits the proliferation and viability of HNSCC cells through G1 arrest. Three human HNSCC cell lines (HN6, HN30, and CAL27) were used to detect the inhibitory

effect of neferine on cell proliferation via CCK-8 assays. The cell viabilities of HN6, HN30, and CAL27 were significantly decreased in a concentration- and time-dependent manner following treatment with neferine (Fig. 1A). The IC_{50} values at 72 h were 13.13, 21.74, and 22.54 μM in HN6, HN30, and CAL27 cells, respectively. Similarly, the colony forming capacity was inhibited by neferine, in a concentration-dependent manner (Fig. 1B). Hence, the cell cycle distribution was examined via flow cytometry, which revealed that neferine induced an obvious G1 cell cycle arrest in three cell lines. In fact, the percentage of cells in the G1 phase increased from 44.86% (0 μM) to 63.78% (20 μM), whereas that in the S phase decreased from 41.42% (0 μM) to 22.14% (20 μM) in the HN6 cells. Similar results were observed in the other two cell lines (Figs. 1C and S1A). Collectively, these results indicated that neferine exerted its inhibitory effect by inducing cell cycle arrest in HNSCC cells.

To investigate the effects of neferine on HNSCC cell motility, a scratch healing assay and Transwell assay were performed. Neferine suppressed the healing and migration of HNSCC cells in a concentration-dependent manner (Fig. S1B and C). Overall, these results indicated that neferine exhibited potential anticancer properties.

Neferine induces ROS and activates the ASK1/JNK pathway to promote apoptosis in HNSCC cells. To investigate the underlying mechanisms of neferine-induced cytotoxicity in HNSCC cells, the number of apoptotic HN6, HN30, and CAL27 cells was quantified via flow cytometry using FITC Annexin V/PI staining in the presence or absence of neferine. The results revealed that neferine increased apoptosis from 7.51% (0 μM) to 11.81% (5 μM), 27.90% (10 μM), 49.10% (15 μM), and 64.70% (20 μM) in HN6 cells (Fig. 1D). Similar trends were observed in CAL27 and HN30 cells (Figs. 1D and S2A). In addition, neferine decreased the Bcl-2/BAX ratio and triggered the cleavage of caspase-8, caspase-9, caspase-3, and PARP-1 in a concentration- and time-dependent manner (Figs. 1E and S2B). Collectively, these results indicated that neferine effectively induced apoptosis in HNSCC cells.

ROS are a vital inducer of apoptosis (25,26). Therefore, to explore whether the neferine-induced apoptosis was associated with ROS hypergeneration, the ROS levels were measured via flow cytometry using the oxidation-sensitive fluorescent probe DCF. The mean fluorescence intensity of DCF in the neferine-treated HN30 cells increased by 2.62-fold (10 μM) and 3.01-fold (20 μM) compared to that in the control cells (0 μM). Similar results were observed in CAL27 cells, but not in HN6 (Fig. 2A). The fluorescence microscopy images also confirmed an increase in ROS (Fig. 2B). Moreover, considering that ROS reportedly activates the ASK1/JNK signaling pathway to induce mitochondrial apoptosis via the caspase family and Beclin-1-dependent autophagy (27,28), the expression of ASK1/JNK protein in HN30 and CAL27 cells treated with neferine was also detected. It was revealed that neferine upregulated the phosphorylation of ASK1/JNK in a concentration- and time-dependent manner; however, it did not alter the overall ASK1/JNK expression (Fig. 2C). These results indicated that neferine induced ROS generation, which activated the ASK1/JNK pathway to induce apoptosis in HNSCC cells.

Neferine promotes the generation of autophagosomes while inhibiting autophagy influx. A previous study revealed that autophagy can be stimulated by ROS (26). Considering the indistinct interaction between apoptosis and autophagy, the effect of neferine on autophagy in the HNSCC cell lines was also explored. Specifically, Beclin-1 expression was analyzed owing to its important role in the initial steps of canonical autophagy (29). The results revealed that Beclin-1 was increased in the neferine-treated HN30 and CAL27 cells in a concentration- and time-dependent manner (Figs. 3A and S3A). Moreover, LC3 and p62 represent universal markers for autophagy. Specifically, the conversion of LC3-I to LC3-II increases as autophagosomes mature, whereas p62 is degraded in the autolysosome, causing its abundance to decrease with activated autophagic flux (29). Our results revealed the increased conversion of LC3-I to the LC3-II isoform in the neferine-treated HN30 and CAL27 cells (Figs. 3A and S3A), indicating the maturation of the autophagosomes. However, the p62 protein level also increased. TEM revealed that treatment with neferine increased the number of vacuoles containing degradative cytoplasmic materials in the HN30 and CAL27 cells (Fig. 3B).

To further explore the influence of neferine on autophagy, the autophagic flux was directly monitored using an autophagosome-lysosome fusion inhibitor, chloroquine (29). First, the LC3-II levels in HN30 and CAL27 cells during neferine treatment, with or without chloroquine were examined. Co-treatment increased the LC3-II levels more significantly than chloroquine alone (Figs. 3C and S3B), indicating that neferine promoted autophagosome biosynthesis. However, p62 abundance was not further increased in the presence of chloroquine, suggesting that the neferine-induced upregulation of p62 may be caused via the inhibition of autophagic degradation (Figs. 3C and S3B). To further verify these results, the autophagic flux was also examined by transfecting double-labeled fluorescent LC3 adenovirus (mCherry-GFP-LC3) (30,31) into HN30 and CAL27 cells. Colocalization (yellow) of both GFP (green) and mCherry (red) fluorescence implied the generation of autophagosomes, whereas red puncta ($mCherry^+$ GFP^-) indicated the generation of autolysosomes. The treatment of neferine (5 μM and 12 h) was not presented, because the autophagosomes (fluorescent puncta) were little or blurry. The treatment of neferine (10 μM and 24 h) was an appropriate condition, since autophagosomes were obvious for counting and to perform the statistical analysis. As revealed in Fig. 3D and E, the yellow puncta were increased without an accompanying increase in the red puncta, indicating that the autophagic flux was blocked. These results indicated that neferine induced autophagosome biosynthesis while inhibiting autophagic flux at the final degradation step in HNSCC cell lines.

Neferine-induced apoptosis is partially mediated by autophagy influx suppression in HNSCC cells. To explore the functional relationship between neferine-induced autophagy and apoptosis, HN30 and CAL27 cells were treated with neferine (20 μM) in the presence or absence of chloroquine (10 μM) and apoptosis analysis was performed. Treatment with chloroquine alone had no obvious effect on cell apoptosis or viability in both cell lines (Fig. 4A and B). However, chloroquine further amplified neferine-induced cell cytotoxicity (Fig. 4A) and moderately

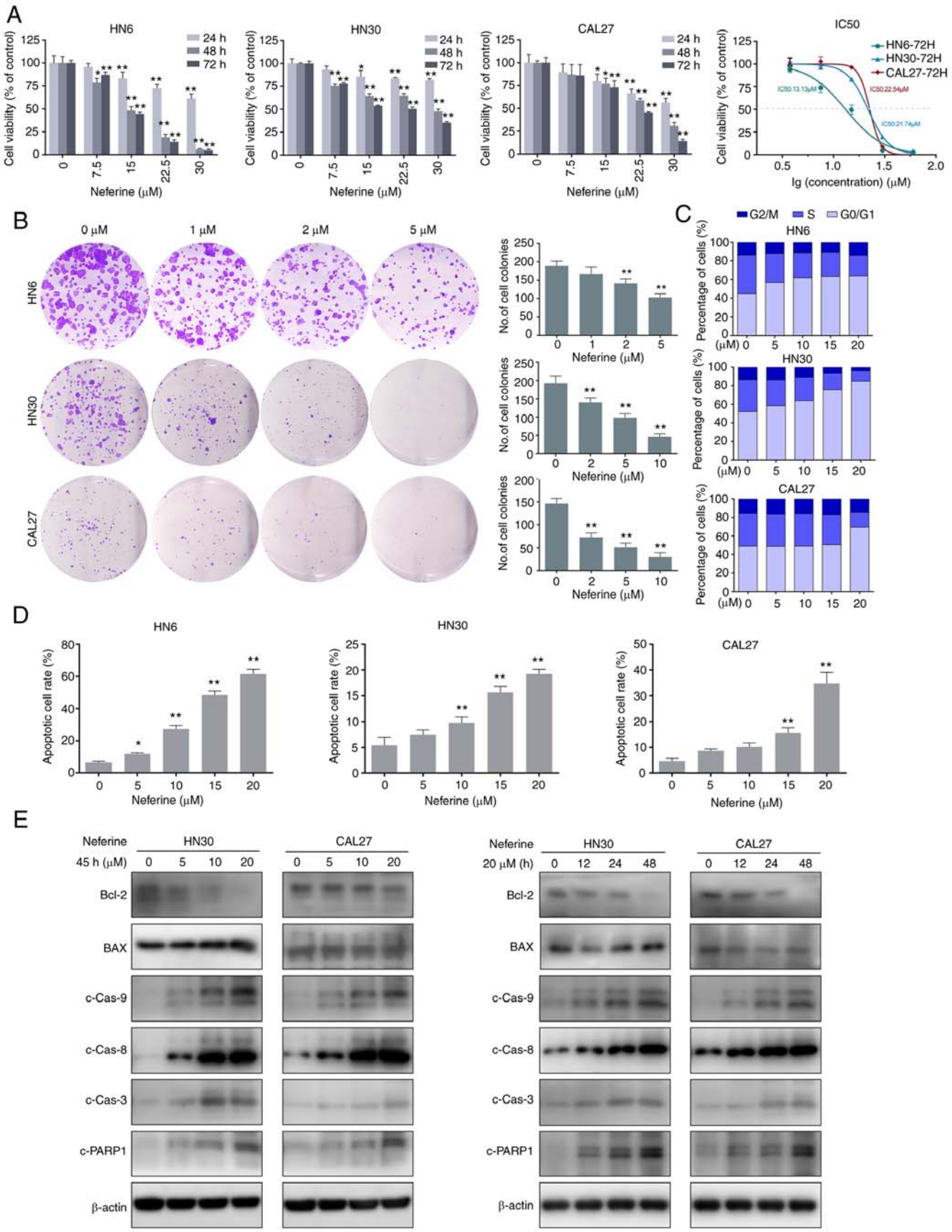

Figure 1. Neferine reduces cell viability and induces apoptosis in HNSCC cells. (A) Histograms present the cell viabilities of HN6, HN30, and CAL27 cells following treatment with neferine. Line chart depicts the IC_{50} values at 72 h in HN6, HN30, and CAL27 cells. (B) Plate colony formation assay showing the inhibitory effect of neferine on HNSCC cells with the indicated concentrations. (C) Cell cycle distribution of the cells treated with various concentrations of neferine for 24 h, as examined via flow cytometry. (D) Flow cytometric analysis of early and late apoptosis in the HN6, HN30, and CAL37 cells treated with neferine. (E) Apoptosis-related protein expression in the HN30 and CAL37 cells treated with neferine confirmed by western blot analysis. Left panel, HN30 and CAL37 cells treated with the indicated concentrations of neferine for 48 h. Right panel, HN30 and CAL37 cells treated with neferine (20 μM) for the indicated durations of time. *P<0.05 and **P<0.01. HNSCC, head and neck squamous cell carcinoma.

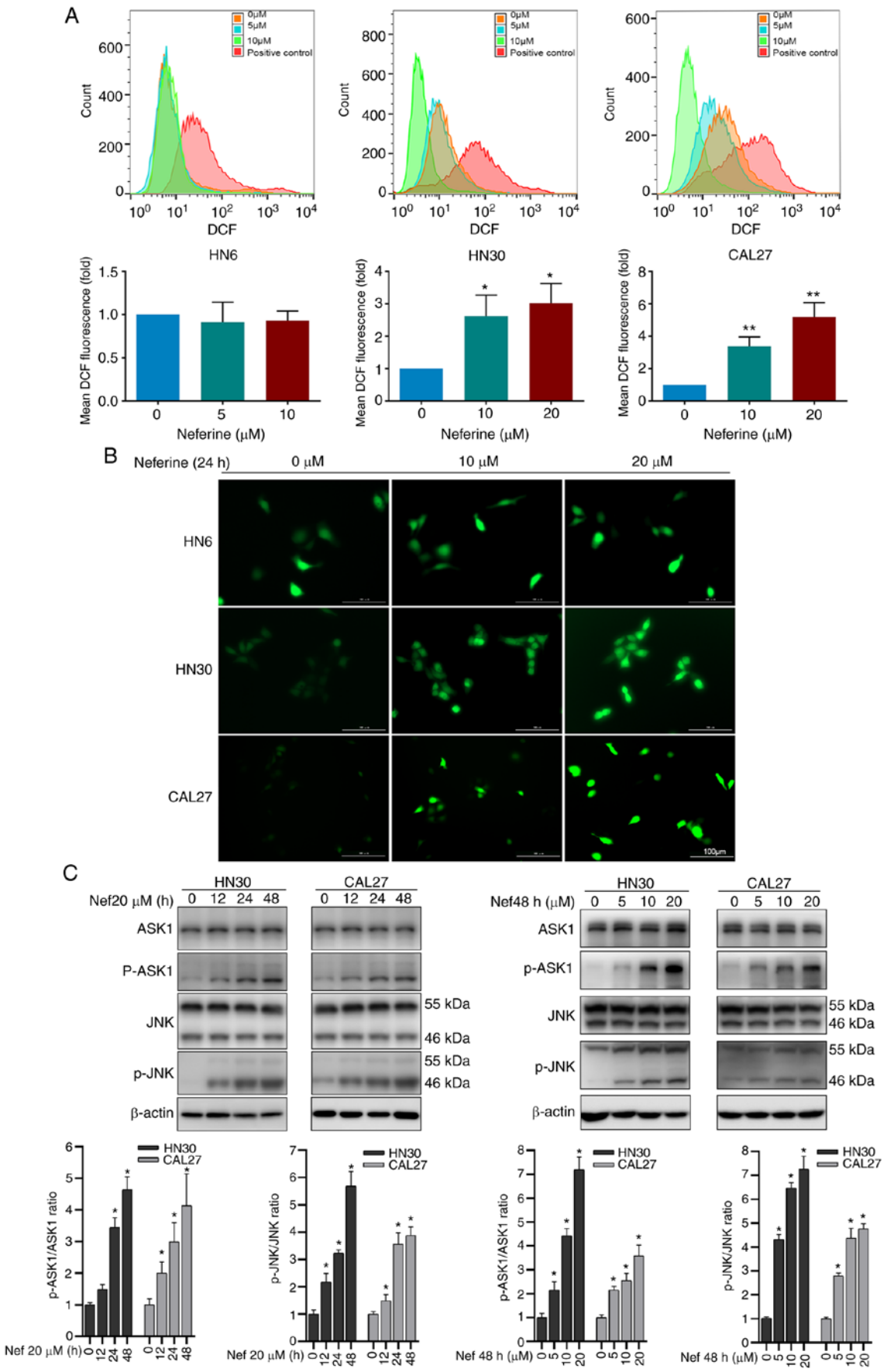

Figure 2. Neferine induces ROS hypergeneration and activates the ASK1/JNK pathway to promote apoptosis and autophagosome biosynthesis in HNSCC cells. (A) Flow cytometric analysis and histograms depicting ROS abundance in HNSCC cells treated with neferine for 24 h using the oxidation-sensitive fluorescent probe DCF. (B) Fluorescence images demonstrating ROS abundance following neferine treatment. (C) Western blotting of ASK1/JNK signaling pathway proteins in HNSCC cells treated with neferine in different conditions (0, 5, 10 and 20 μM; 0, 12, 24 and 48 h). *P<0.05 and **P<0.01. HNSCC, head and neck squamous cell carcinoma; ROS, reactive oxygen species; DCF, dichlorofluorescein.

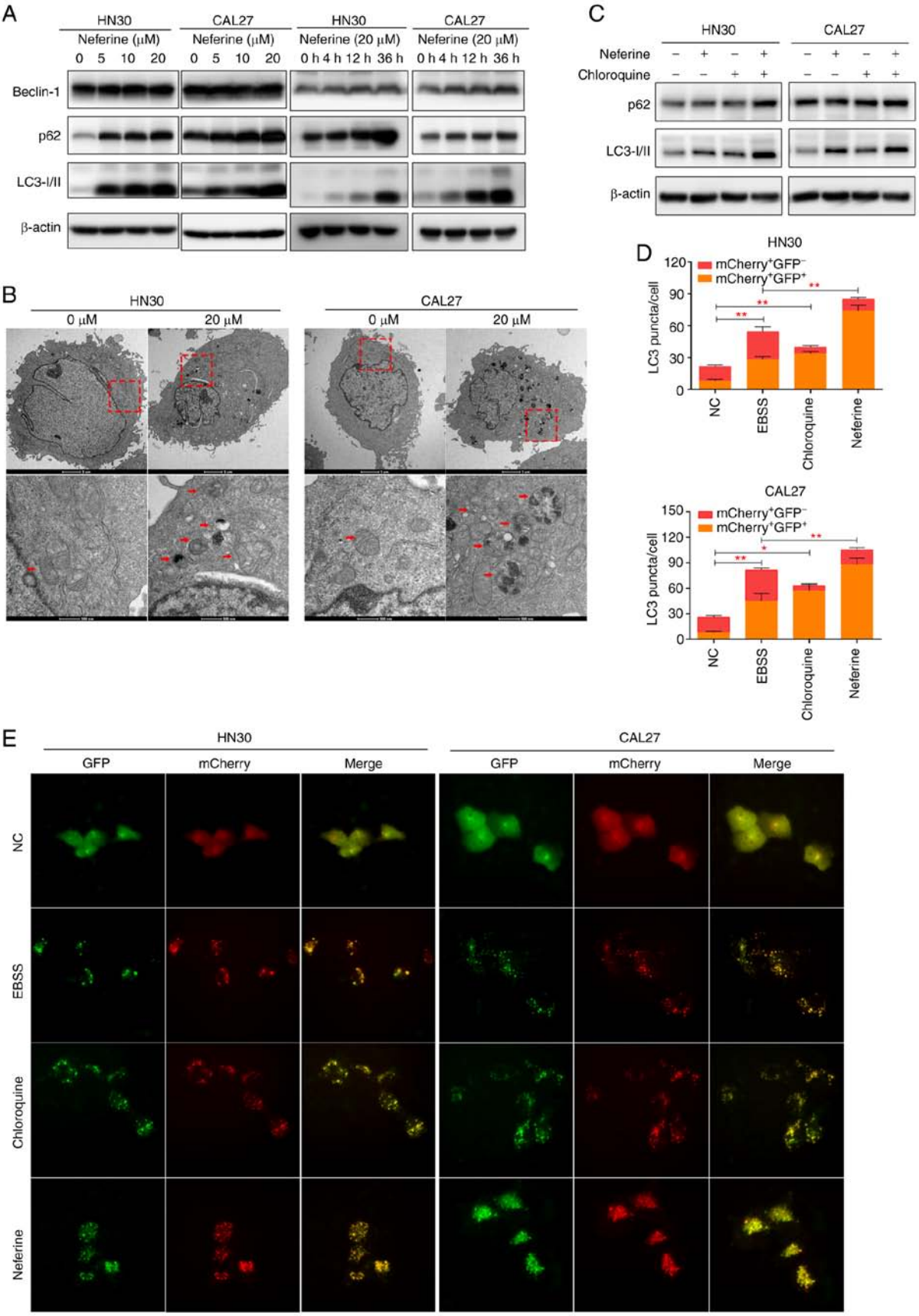

Figure 3. Neferine promotes the generation of autophagosomes while inhibiting autophagic influx in head and neck squamous cell carcinoma cells. (A) The expression of Beclin-1, p62, and LC3 as analyzed by western blotting in HN30 and CAL27 cells following treatment with neferine at the indicated concentrations and durations of time. (B) Transmission electron microscopy of the neferine-treated (20 μM) cells depicting the number of vacuoles containing cytoplasmic materials and multivesicular bodies, a characteristic feature of degradative autophagic vacuoles. (C) Western blot analysis of p62 and LC3 expression in the HN30 and CAL27 cells concomitantly treated with neferine (20 μM) and chloroquine (10 μM). (D and E) Autophagic flux examined through double-labeled fluorescent LC3 adenovirus (mCherry$^+$GFP$^-$-LC3 and mCherry$^+$GFP$^+$-LC3). Colocalization (yellow) of both GFP (green) and mCherry (red) fluorescence indicated the generation of autophagosomes (neferine 10 μM, 24 h; EBSS 6 h; chloroquine 10 μM, 24 h). *P<0.05 and **P<0.01.

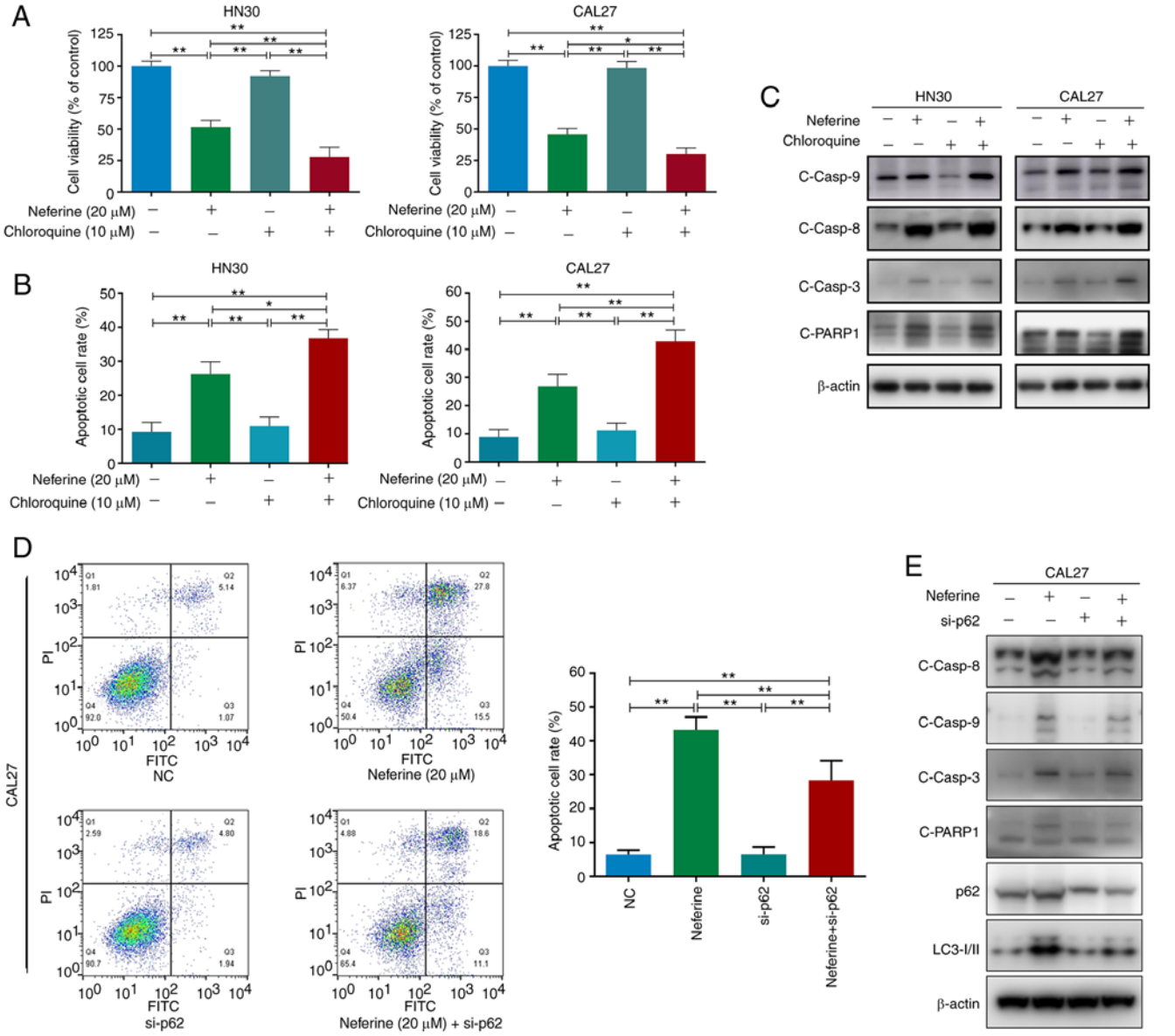

Figure 4. Neferine-induced apoptosis is partially mediated via the accumulation of p62 due to neferine-induced autophagic influx inhibition in head and neck squamous cell carcinoma cells. (A) Cell viability, (B) apoptotic cell rate, and (C) western blot analysis of cleaved caspase-8, caspase-9, caspase-3, and PARP1 in HN30 and CAL27 cells treated with neferine (20 μM) in the presence or absence of chloroquine (10 μM) for 48 h. (D) Flow cytometric analysis of early and late apoptosis and (E) western blot analysis of cleaved caspase-8, caspase-9, caspase-3, PARP1, p62, and LC3 in neferine-treated HN30 and CAL37 cells with or without p62 knockdown. *P<0.05 and **P<0.01. NC, negative control; si-, small interfering.

intensified neferine-induced apoptosis, while inducing further activation of caspase-8, caspase-3, and PARP1 (Figs. 4B and C, and S4A and B). These results indicated that the inhibition of autophagic flux by chloroquine promoted the neferine-induced apoptosis of HN30 and CAL27 cells.

Since neferine was revealed to directly inhibit autophagic flux, it could be concluded that the neferine-induced apoptosis was partially enhanced by neferine-induced autophagic influx inhibition. In addition, considering that the expression of cleaved caspase-9 showed no noticeable difference between the neferine group and the neferine + chloroquine group (Figs. 4C and S4B), the further pro-apoptotic effects may be executed by caspase-8, but not caspase-9.

Accumulation of p62 due to neferine-induced autophagy influx inhibition promotes apoptosis in HNSCC cells. Previous studies have revealed that p62 acts as a 'bridge' between apoptosis and autophagy (32,33). Moreover, it was observed that the neferine-induced autophagic flux inhibition caused an increase in the p62 level (Fig. 3). Hence, to investigate the role of p62 in the neferine-induced crosstalk between apoptosis and autophagy, the expression of p62 was downregulated in CAL27 cells, the CAL27 cells were treated with neferine, and subsequently the level of apoptosis was quantified. Flow cytometric analysis revealed that p62 knockdown alleviated the neferine-induced apoptosis (from 43.3 to 29.7%) in CAL27 cells (Fig. 4D). Moreover, the cleavage of specific apoptosis-related proteins, caspase-8, caspase-3, and PARP1, was decreased; however, the same effect was not observed for cleaved caspase-9 (Figs. 4E and S4C). These results confirmed that the neferine-induced accumulation of p62 activated caspase-8 to promote apoptosis in HNSCC cells.

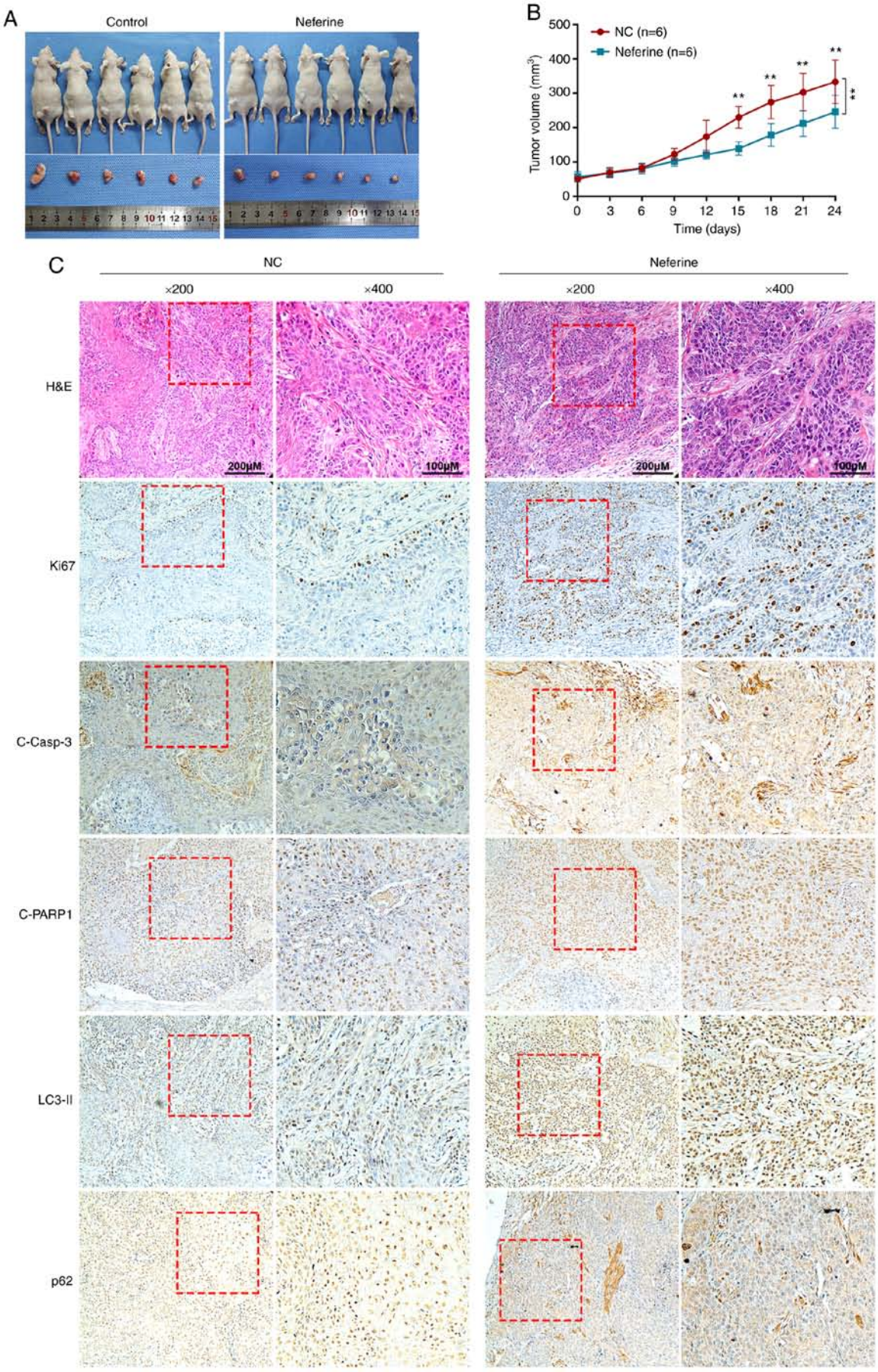

Figure 5. Neferine inhibits the growth of head and neck squamous cell carcinoma by inducing apoptosis and autophagy *in vivo*. (A) Representative images of xenografts constructed by CAL27 cells, treated with vehicle or neferine. (B) The line chart depicts the growth rate of tumors treated with neferine compared to the control. (C) H&E staining and immunohistochemical staining of Ki67, cleaved caspase-3, cleaved PARP1, LC3, and p62 in xenograft tumor tissues treated with neferine or vehicle. $^{**}P<0.01$.

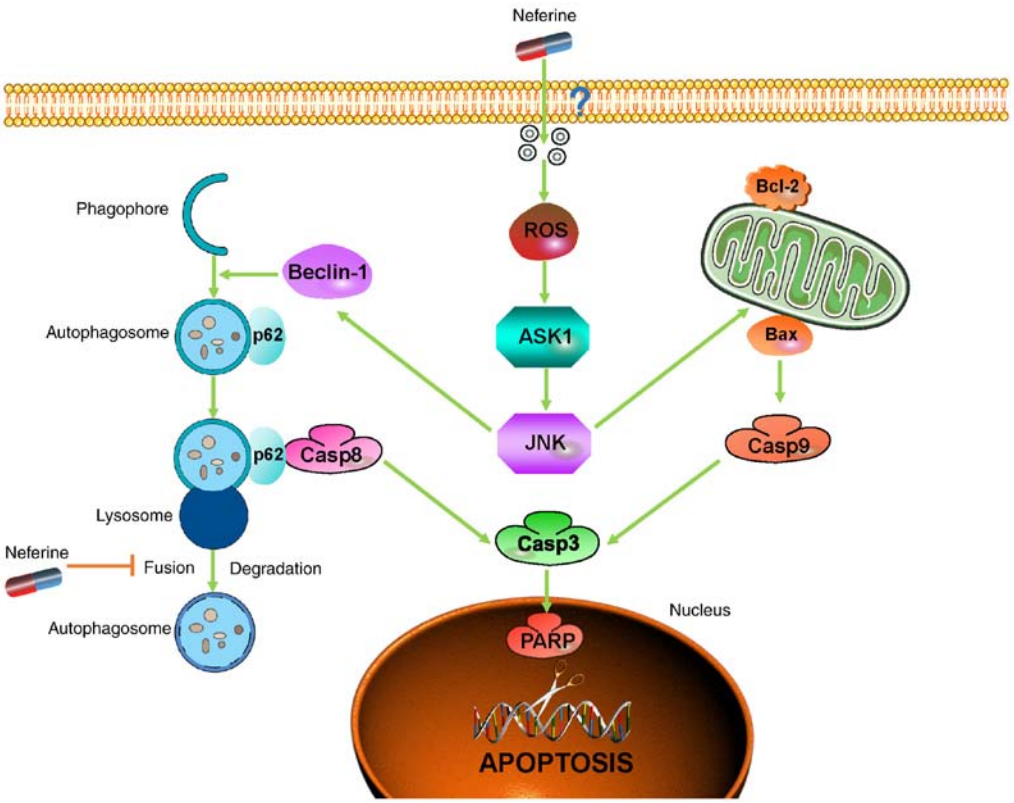

Figure 6. Neferine promotes head and neck squamous cell carcinoma cell apoptosis through the accumulation of p62/SQSTM1 caused by autophagic flux inhibition. (The precise mechanism about how neferine crosses the cell membrane was unknown, thus a '?' was added in the graphic abstract).

Neferine inhibits the growth of HNSCC cells by inducing apoptosis and autophagy in vivo. Next, to examine the effects of neferine *in vivo* a murine xenograft model with CAL27 cells was used. The tumor volumes following treatment with neferine were significantly smaller than that of the control. The growth rate of tumors treated with neferine was also slower than that of the control (Fig. 5A and B). Furthermore, the immunohistochemical staining of xenograft tumor tissues (Fig. 5C) revealed that treatment with neferine decreased the expression of Ki67, a marker of cell proliferation. In addition, neferine increased the expression of cleaved caspase-3 and cleaved PARP1 in the nucleus, indicating that neferine induced the apoptosis of xenograft tumors. In accordance with the *in vitro* results, neferine also increased the level of LC3-II and p62, indicating that neferine induced autophagosome generation and inhibited autophagy influx *in vivo*.

Discussion

Neferine is a plant-derived reagent that induces higher toxicity in cancer cells compared to non-transformed cells (15). It has also been reported to induce ovarian and hepatoma carcinoma cell apoptosis and autophagy (16,34); however, one study reported contradictory results indicating that neferine functions as an autophagy inhibitor in ARPE-19 (35). In addition, neither the effects of neferine on HNSCC nor the reciprocal interaction between apoptosis and autophagy induced by neferine had been previously characterized. Hence, the present study aimed to elucidate the influence of neferine on autophagy and apoptosis in HNSCC

Numerous studies have reported the inhibitory effects elicited by neferine on cell proliferation, growth, migration, and angiogenesis in different tumors (10,13,16). In fact, some studies have even focused on ROS production as well as apoptosis and autophagy induction (15,34). However, most of these previous studies were independent studies that did not evaluate autophagic flux specifically. Herein, a multidimensional evaluation was conducted and the pharmacological effect of neferine was revealed to be undoubtedly versatile. First, it was revealed that neferine inhibited the viability and colony formation of cancer cells while arresting HNSCC cells in the G1/S phase. Similar results were also reported in ovarian carcinoma via the downregulation of cyclin E1 (16). Neferine was also revealed to suppress the healing and migration of HNSCC cells, further highlighting its potential anticancer properties, which were verified in an *in vivo* murine xenograft model. Furthermore, it was determined that neferine induced apoptosis and autophagy while increasing the level of ROS production and the activation of the ASK1/JNK pathway. Indeed, ROS served as an initiator for the activation of ASK1 (oxidative stress sensor) and JNK. Specifically, with the activation of JNK, the mitochondrial apoptosis induced by Bcl-2 inhibition and the canonical autophagy induced by JNK/Beclin-1 were sequential occurrences (36,37). Hence, neferine-induced ROS likely served as an upstream effector for apoptosis and autophagy. Moreover, the results indicated that neferine-induced autophagosome biogenesis was determined by the Beclin1-dependent canonical autophagy pathway. It was also a limitation of this study that the effect of ROS on the ASK1/JNK pathway by further interfering with ROS was absent. The treatment of

neferine increased the level of ROS in HN30 and Cal27 cells, but not in HN6 cells. Although these 3 cell lines belong to head and neck squamous cell carcinoma, they have different genetic backgrounds and anatomical origins. Cell line disparity was revealed when the effect of neferine was evaluated. In addition, this result revealed that the inhibiting effects of neferine on HNSCC were not only through the ROS pathway, but also other mechanisms (for example, by the autophagic flux inhibition).

Autophagy serves as a crucial mechanism for the degradation of harmful cellular components to mediate metabolic adaptation and maintain energy homeostasis (38). Several studies have revealed that autophagy exhibits a paradoxical role, having either tumor-promoting or tumor-suppressive effects on carcinoma (39,40). Moreover, the inhibition of autophagy is regarded as a universal target for anticancer therapy (41). In our research, neferine functioned as a double-edged sword for autophagy in HNSCC. It was revealed that neferine induced autophagosome generation, while also inhibiting autophagic flux at the autophagosome degradation step as evidenced by the increased conversion of LC3-I to LC3-II and the accumulation of p62.

p62/SQSTM1 is involved in the formation of autophagosomes and is degraded by lysosomal proteases along with autophagosomes (42). Hence, the inhibition of autophagic flux by neferine caused the accumulation of p62. p62 is a scaffold protein composed of five domains that organize signal trafficking at critical points to regulate cell death and survival (43,44). Specifically, the UBA domain of p62 interacts with ubiquitinated proteins, thus, p62 recruits and oligomerizes important signaling molecules (44). Moreover, p62 reportedly provides a signal-organizing interface to recruit poly-ubiquitinated caspase-8 and subsequently activate caspase-8 (33). The present results revealed that neferine induced the accumulation of p62, which subsequently enhanced neferine-induced apoptosis. This was also confirmed by downregulation of p62, however, the absence of experiments using a caspase-8 inhibitor is a limitation of our study. Hence, collectively, the results indicated that p62 may function as a bridge between the autophagy and apoptosis induced by neferine.

When treated with reagents that induce proteasome inhibition or endoplasmic reticular stress, cells can activate apoptosis directly through caspase-8 (45). This mechanism is strengthened by the function of LC-3 and p62 (46,47). Therefore, a novel mechanism is proposed for neferine in which the accumulation of p62 by autophagic influx inhibition promotes apoptosis through the activation of caspase-8, independent of ROS, in HNSCC cells. The involvement of p62 in neferine-induced cell apoptosis through caspase-8 activation broadened our understanding of the mechanism responsible for neferine-induced cell death. Moreover, the crosstalk between autophagy and apoptosis may have required the participation of p62 as a conjunction point in neferine-induced cell death. Considering that the activation of caspase-8 was accompanied with the accumulation of p62, it is plausible that caspase-8 may interact with p62 at the autophagosome surface during neferine treatment.

In conclusion, considering the present findings of increased apoptosis and interrupted autophagic flux, our study clarified the underlying pro-apoptotic mechanism of neferine in HNSCC through the inhibition of autophagic influx mediated by p62, thereby providing new insights into the crosstalk between apoptosis and autophagy while highlighting neferine as a potential agent to improve the prognosis of HNSCC patients (Fig. 6).

Acknowledgements

Not applicable.

Funding

This work was supported by the National Natural Science Foundation of China (grant no. 81570949).

Availability of data and materials

All data generated or analyzed during this study are included in this published article.

Authors' contributions

FZ, XL, XT, YHa and JJ performed the research and analyzed the results. FZ, YL, and ZL developed the methodology and discussed the results. FZ, CM and YHe designed the research, wrote the paper, and supervised the study. All authors read and approved the final manuscript.

Ethics approval and consent to participate

The animal experiments were approved by the Ethics Review Board at the Shanghai Ninth People's Hospital (Shanghai, China).

Patient consent for publication

Not applicable.

Competing interests

The authors declare that they have no competing interests.

References

1. Vigneswaran N and Williams MD: Epidemiologic trends in head and neck cancer and aids in diagnosis. Oral Maxillofac Surg Clin North Am 26: 123-141, 2014.
2. Bray F, Ferlay J, Soerjomataram I, Siegel RL, Torre LA and Jemal A: Global cancer statistics 2018: GLOBOCAN estimates of incidence and mortality worldwide for 36 cancers in 185 countries. CA Cancer J Clin 68: 394-424, 2018.
3. Johnson DE, Burtness B, Leemans CR, Lui VWY, Bauman JE and Grandis JR: Head and neck squamous cell carcinoma. Nat Rev Dis Primers 6: 92, 2020.
4. Yamano Y, Uzawa K, Saito K, Nakashima D, Kasamatsu A, Koike H, Kouzu Y, Shinozuka K, Nakatani K, Negoro K, *et al*: Identification of cisplatin-resistance related genes in head and neck squamous cell carcinoma. Int J Cancer 126: 437-449, 2010.
5. GBD 2015 Mortality and Causes of Death Collaborators: Global, regional, and national life expectancy, all-cause mortality, and cause-specific mortality for 249 causes of death, 1980-2015: A systematic analysis for the Global Burden of Disease Study 2015. Lancet 388: 1459-1544, 2016.
6. Qian JQ: Cardiovascular pharmacological effects of bisbenzylisoquinoline alkaloid derivatives. Acta Pharmacol Sin 23: 1086-1092, 2002.

7. Zhao L, Wang X, Chang Q, Xu J, Huang Y, Guo Q, Zhang S, Wang W, Chen X and Wang J: Neferine, a bisbenzylisoquinline alkaloid attenuates bleomycin-induced pulmonary fibrosis. Eur J Pharmacol 627: 304-312, 2010.
8. Sugimoto Y, Furutani S, Itoh A, Tanahashi T, Nakajima H, Oshiro H, Sun S and Yamada J: Effects of extracts and neferine from the embryo of *Nelumbo nucifera* seeds on the central nervous system. Phytomedicine 15: 1117-1124, 2008.
9. Erdogan S and Turkekul K: Neferine inhibits proliferation and migration of human prostate cancer stem cells through p38 MAPK/JNK activation. J Food Biochem 44: e13253, 2020.
10. Zhang X, Liu Z, Xu B, Sun Z, Gong Y and Shao C: Neferine, an alkaloid ingredient in lotus seed embryo, inhibits proliferation of human osteosarcoma cells by promoting p38 MAPK-mediated p21 stabilization. Eur J Pharmacol 677: 47-54, 2012.
11. Deng G, Zeng S, Ma J, Zhang Y, Qu Y, Han Y, Yin L, Cai C, Guo C and Shen H: The anti-tumor activities of Neferine on cell invasion and oxaliplatin sensitivity regulated by EMT via Snail signaling in hepatocellular carcinoma. Sci Rep 7: 41616, 2017.
12. Poornima P, Weng CF and Padma VV: Neferine, an alkaloid from lotus seed embryo, inhibits human lung cancer cell growth by MAPK activation and cell cycle arrest. Biofactors 40: 121-131, 2014.
13. Xue F, Liu Z, Xu J, Xu X, Chen X and Tian F: Neferine inhibits growth and migration of gastrointestinal stromal tumor cell line GIST-T1 by up-regulation of miR-449a. Biomed Pharmacother 109: 1951-1959, 2019.
14. Liang HX, Sun LB and Liu NJ: Neferine inhibits proliferation, migration and invasion of U251 glioma cells by down-regulation of miR-10b. Biomed Pharmacother 109: 1032-1040, 2019.
15. Xu L, Zhang X, Li Y, Lu S, Lu S, Li J, Wang Y, Tian X, Wei JJ, Shao C and Liu Z: Neferine induces autophagy of human ovarian cancer cells via p38 MAPK/ JNK activation. Tumour Biol 37: 8721-8729, 2016.
16. Zhang Q, Li Y, Miao C, Wang Y, Xu Y, Dong R, Zhang Z, Griffin BB, Yuan C, Yan S, *et al*: Anti-angiogenesis effect of Neferine via regulating autophagy and polarization of tumor-associated macrophages in high-grade serous ovarian carcinoma. Cancer Lett 432: 144-155, 2018.
17. Vakifahmetoglu-Norberg H, Xia HG and Yuan J: Pharmacologic agents targeting autophagy. J Clin Invest 125: 5-13, 2015.
18. Mizushima N, Yoshimori T and Levine B: Methods in mammalian autophagy research. Cell 140: 313-326, 2010.
19. Cheng Y, Ren X, Hait WN and Yang JM: Therapeutic targeting of autophagy in disease: Biology and pharmacology. Pharmacol Rev 65: 1162-1197, 2013.
20. Su M, Mei Y and Sinha S: Role of the Crosstalk between Autophagy and Apoptosis in Cancer. J Oncol 2013: 102735, 2013.
21. Zhong LP, Pan HY, Zhou XJ, Ye DX, Zhang L, Yang X, Chen WT and Zhang ZY: Characteristics of a cancerous cell line, HIOEC-B(a)P-96, induced by benzo(a)pyrene from human immortalized oral epithelial cell line. Arch Oral Biol 53: 443-452, 2008.
22. Lucocq JM and Hacker C: Cutting a fine figure: On the use of thin sections in electron microscopy to quantify autophagy. Autophagy 9: 1443-1448, 2013.
23. Eskelinen EL, Reggiori F, Baba M, Kovacs AL and Seglen PO: Seeing is believing: The impact of electron microscopy on autophagy research. Autophagy 7: 935-956, 2011.
24. Pankiv S, Lamark T, Bruun JA, Overvatn A, Bjorkoy G and Johansen T: Nucleocytoplasmic shuttling of p62/SQSTM1 and its role in recruitment of nuclear polyubiquitinated proteins to promyelocytic leukemia bodies. J Biol Chem 285: 5941-5953, 2010.
25. Martindale JL and Holbrook NJ: Cellular response to oxidative stress: Signaling for suicide and survival. J Cell Physiol 192: 1-15, 2002.
26. Chen Y and Gibson SB: Is mitochondrial generation of reactive oxygen species a trigger for autophagy? Autophagy 4: 246-248, 2008.
27. Liu J and Lin A: Role of JNK activation in apoptosis: A double-edged sword. Cell Res 15: 36-42, 2005.
28. Tang D, Kang R, Zeh HJ III and Lotze MT: High-mobility group box 1, oxidative stress, and disease. Antioxid Redox Signal 14: 1315-1335, 2011.
29. Klionsky DJ, Abdelmohsen K, Abe A, Abedin MJ, Abeliovich H, Acevedo Arozena A, Adachi H, Adams CM, Adams PD, Adeli K, *et al*: Guidelines for the use and interpretation of assays for monitoring autophagy (3rd edition). Autophagy 12: 1-222, 2016.
30. Kimura S, Noda T and Yoshimori T: Dissection of the autophagosome maturation process by a novel reporter protein, tandem fluorescent-tagged LC3. Autophagy 3: 452-460, 2007.
31. Pankiv S, Clausen TH, Lamark T, Brech A, Bruun JA, Outzen H, Øvervatn A, Bjørkøy G and Johansen T: p62/SQSTM1 binds directly to Atg8/LC3 to facilitate degradation of ubiquitinated protein aggregates by autophagy. J Biol Chem 282: 24131-24145, 2007.
32. Philip NH, DeLaney A, Peterson LW, Santos-Marrero M, Grier JT, Sun Y, Wynosky-Dolfi MA, Zwack EE, Hu B, Olsen TM, *et al*: Activity of uncleaved caspase-8 controls anti-bacterial immune defense and TLR-induced cytokine production independent of cell death. PLoS Pathog 12: e1005910, 2016.
33. Zhang YB, Gong JL, Xing TY, Zheng SP and Ding W: Autophagy protein p62/SQSTM1 is involved in HAMLET-induced cell death by modulating apotosis in U87MG cells. Cell Death Dis 4: e550, 2013.
34. Poornima P, Quency RS and Padma VV: Neferine induces reactive oxygen species mediated intrinsic pathway of apoptosis in HepG2 cells. Food Chem 136: 659-667, 2013.
35. Xu T, Singh D, Liu J, Li H, Peng S, Rizzolo LJ and Wang SB: Neferine, is not inducer but blocker for macroautophagic flux targeting on lysosome malfunction. Biochem Biophys Res Commun 495: 1516-1521, 2018.
36. Zhao Q, Liu Y, Zhong J, Bi Y, Liu Y, Ren Z, Li X, Jia J, Yu M and Yu X: Pristimerin induces apoptosis and autophagy via activation of ROS/ASK1/JNK pathway in human breast cancer in vitro and in vivo. Cell Death Discov 5: 125, 2019.
37. Ma L, Wei J, Wan J, Wang W, Wang L, Yuan Y, Yang Z, Liu X and Ming L: Low glucose and metformin-induced apoptosis of human ovarian cancer cells is connected to ASK1 via mitochondrial and endoplasmic reticulum stress-associated pathways. J Exp Clin Cancer Res 38: 77, 2019.
38. Li T, Su L, Zhong N, Hao X, Zhong D, Singhal S and Liu X: Salinomycin induces cell death with autophagy through activation of endoplasmic reticulum stress in human cancer cells. Autophagy 9: 1057-1068, 2013.
39. Rosenfeldt MT and Ryan KM: The role of autophagy in tumour development and cancer therapy. Expert Rev Mol Med 11: e36, 2009.
40. Kondo Y and Kondo S: Autophagy and cancer therapy. Autophagy 2: 85-90, 2006.
41. Sui X, Chen R, Wang Z, Huang Z, Kong N, Zhang M, Han W, Lou F, Yang J, Zhang Q, *et al*: Autophagy and chemotherapy resistance: A promising therapeutic target for cancer treatment. Cell Death Dis 4: e838, 2013.
42. Ichimura Y and Komatsu M: Selective degradation of p62 by autophagy. Semin Immunopathol 32: 431-436, 2010.
43. Moscat J, Diaz-Meco MT and Wooten MW: Signal integration and diversification through the p62 scaffold protein. Trends Biochem Sci 32: 95-100, 2007.
44. Moscat J and Diaz-Meco MT: p62 at the crossroads of autophagy, apoptosis, and cancer. Cell 137: 1001-1004, 2009.
45. Hou W, Han J, Lu C, Goldstein LA and Rabinowich H: Autophagic degradation of active caspase-8: A crosstalk mechanism between autophagy and apoptosis. Autophagy 6: 891-900, 2010.
46. Young MM, Takahashi Y, Khan O, Park S, Hori T, Yun J, Sharma AK, Amin S, Hu CD, Zhang J, *et al*: Autophagosomal membrane serves as platform for intracellular death-inducing signaling complex (iDISC)-mediated caspase-8 activation and apoptosis. J Biol Chem 287: 12455-12468, 2012.
47. Pan JA, Fan Y, Gandhirajan RK, Madesh M and Zong WX: Hyperactivation of the mammalian degenerin MDEG promotes caspase-8 activation and apoptosis. J Biol Chem 288: 2952-2963, 2013.